IEEE Access
Multidisciplinary | Rapid Review | Open Access Journal

Received January 9, 2021, accepted January 20, 2021, date of publication January 25, 2021, date of current version February 4, 2021.

Digital Object Identifier 10.1109/ACCESS.2021.3054065

Using Rear Smartphone Cameras as Sensors for Measuring Heart Rate Variability

GENXUAN ZHANG[1,2], SAI ZHANG[1], YIMING DAI[1], AND BO SHI[1,2]
[1]School of Medical Imaging, Bengbu Medical College, Bengbu 233030, China
[2]Anhui Key Laboratory of Computational Medicine and Intelligent Health, Bengbu Medical College, Bengbu 233030, China

Corresponding author: Bo Shi (shibo@bbmc.edu.cn)

This work was supported in part by the "512" Outstanding Talents Fostering Project of Bengbu Medical College under Grant 2020-42-3-12, in part by the Scientific Research Innovation Project of Bengbu Medical College under Grant BYKC201905, and in part by the Natural Science Foundation of Bengbu Medical College under Grant BYKY2019023ZD.

ABSTRACT The measurement of heart rate variability (HRV) is the preferred method for assessing the function of the autonomic nervous system (ANS). Traditional HRV detection requires an electrocardiogram (ECG) or photoelectric sensor. In this paper, we propose a new method for HRV measurement using a rear smartphone camera as a sensor. Video signals from the fingertips of 24 college students were acquired using the rear camera of an HTC M8d smartphone. ECG signals were simultaneously recorded as reference. The video signals were converted into single-frame image sequences over time. Each image frame was transformed into point data through superpositioning of pixel color attribute values and averaging according to space. The point data were sorted by time to obtain a photoplethysmogram (PPG). Finally, the Hilbert transform was used to extract the pulse-to-pulse interval and the R-to-R interval for the PPG and ECG, respectively. Sixteen HRV parameters (mean HR, max HR, min HR, SDNN, RMSSD, NN50, pNN50, VLF, LF, HF, TP, LFnu, HFnu, LF/HF, SD1, and SD2) were analyzed. All 16 HRV parameters were highly correlated (all $rs > 0.95$, $ps < 0.05$), and the effect size (ES) differences were small ($ES < 0.175$) for all indices except for RMSSD, HF, and SD1. Compared with the ECG method, the errors of the 13 HRV parameters measured using this method were within acceptable ranges. The results suggest that this technique can be used as a convenient method to assess and quantify ANS activity and balance.

INDEX TERMS Heart rate variability, photoplethysmography, smartphone, camera, video.

I. INTRODUCTION

Over the past decade, the advent of smartphones has revolutionized daily life. Today, smartphones are no longer simple communication tools; they also have many functions, including photography, payment, and entertainment. With advances in electronic technology and cloud computing, healthcare fields will likely be transformed by smartphones. Currently, smartphones can be used for monitoring personal health by measuring physiological parameters, such as glucose [1], immunoglobulin G [2], and serum bilirubin levels [3], blood pressure [4], electrocardiograms (ECGs) [5], and heart rate variability (HRV) [6], using built-in or external sensors. Among these parameters, HRV, which measures small differences in time between successive normal (sinus) cardiac cycles, is recognized as the preferred metric for quantitatively evaluating the function of the autonomic nervous system (ANS) [7]. Numerous articles have reported inverse relationships of HRV parameters to age [8], [9] and exercise [10], [11]. HRV parameters significantly decreases during disease states, such as diabetes [12], hypertension [13], and cancer [14]. Therefore, monitoring HRV parameters offers important reference values for quantitative health assessment and management.

HRV analysis is generally based on two time series, namely, the R-to-R interval (RRI) of an ECG and the pulse-to-pulse interval (PPI) of a photoplethysmogram (PPG) [15]. Studies have shown that time- and frequency-domain HRV parameters analyzed by PPI are negligibly different from those conducted using RRI [16]–[18]. Regardless of the approach, the use of smartphones for HRV measurements requires external or built-in professional sensors and adds use-related costs to the user. In recent years, high-definition cameras have become standard issue in smartphones. Many scholars have used smartphone cameras as sensors for studies on heart rate (HR) monitoring and HRV measurements

The associate editor coordinating the review of this manuscript and approving it for publication was Hasan S. Mir.

using contact or noncontact video PPG (vPPG) technology [19]–[26]. In general, the noncontact vPPG is more convenient in the application of continuous dynamic monitoring, but the measurement accuracy of the contact vPPG is higher. For HR monitoring, the use of the noncontact method meets measurement accuracy requirements. For example, in 2010, Poh *et al.* [19] proposed a method for measuring the HR using blind source separation (BSS) of facial video imaging. When subjects were at rest, the mean value of the HR error was only -0.05 bpm, and the range of 95% of the limits of agreement (LoA) was (−4.6, 4.4) bpm, i.e., nearly medical-grade levels. Measuring the HRV does not require continuous monitoring but does require higher PPI accuracy, which often cannot be met by the noncontact method. Peng *et al*. [6] used contact vPPG to analyze 16 HRV parameters. Compared with the ECG method, 14 parameters were highly correlated ($r > 0.7$, $p < 0.001$), and the errors of seven parameters were within acceptable ranges. Most existing smartphone camera-based HRV analysis methods are algorithmically complex and have limited accuracy. In this study, a simple video processing algorithm is proposed. Compared with the ECG method, the analyzed HRV time- and frequency-domain parameters were highly correlated ($r > 0.95$, $p < 0.001$).

II. METHOD

A. SUBJECTS AND DATA COLLECTION

Twenty-four college students at Bengbu Medical College, China, participated in this study, with 13 male students and 11 female students. Their mean (± standard deviation) age was 20.6 ± 1.0 years, their height was 1.69 ± 0.07 m, their body weight was 61.5 ± 10.4 kg, and they had a body mass index of 21.5 ± 2.7 kg/m^2. None of the subjects had a history of heart disease or hypertension, and they were informed of the purpose and details of the experiment before participating. The study was conducted in accordance with the Declaration of Helsinki, and the protocol was approved by the Ethics Committee of Bengbu Medical College.

Before the tests, we instructed the subjects. They were asked to keep their fingers clean, apply moderate pressure on the smartphone camera, and remain quiet during the test. Approximately 30% of subjects needed to repeat the test two to three times to obtain a satisfactory signal. Signal satisfaction was dependent on whether 95% PPI was extracted. During the experiment, a video signal from the fingertip of an index finger of each subject was obtained using the rear camera of an HTC M8d smartphone (HTC, Taiwan, China) (Figure 1); simultaneously, the ECG signal of the subjects was recorded synchronously using a HeaLink-R211B micro-ECG recorder (HeaLink, Ltd., Bengbu, China) as reference. The rear camera of the HTC M8d was an HTC 4 million UltraPixel camera with the following settings: Full HD 1920 × 1080 video quality and square (1:1) cropping. The slow-motion mode was selected when recording. The sampling rate of the micro-ECG recorder was set at 400 Hz,

FIGURE 1. A video signal of the index fingertip which was obtained by using the rear camera of an HTC M8d smartphone.

and disposable Ag/AgCl ECG electrodes (Junkang, Ltd., Shanghai, China) were used for signal acquisition.

B. VIDEO SIGNAL PROCESSING

The collected fingertip video signals were processed according to the following steps, and a flow chart of the entire process is shown in Figure 2.

First, the acquired video signal is converted to a single-frame image sequence over time. The video signal acquisition time is 120 s for each subject. X is the number of frames of the video. Assuming that the frame rate of the video acquisition is F frames/s, a video of 120 s will be composed of 120*F frame images, and X will be further scaled by a factor of 4 when filmed in 4x slow-motion mode. The frame rate F is 25 frames/s for the HTC M8d smart phone. Thus, X = 12,000 for a video of 120 s taken in 4x slow-motion mode (i.e., 120*25*4).

Second, each frame image in the image sequence is transformed into point data by pixel superposition and averaging according to the space. For any jth frame image, assuming N pixels and the ith pixel color attribute value is $P_j(i)$, the pixel values of all of points are superimposed and averaged such that the average pixel value P_j of this frame image is obtained. The formula is expressed as

$$P_j = \frac{\sum_{i=1}^{N} P_j(i)}{N}. \tag{1}$$

In this manner, the jth frame image is converted from a two-dimensional image to point data; then, X frames of the image is converted to X point data, namely, $P_1, P_2, P_3 \ldots P_x$.

Finally, the PPG pulse wave is obtained by sorting these point data across time.

The waveform of the pulse wave obtained through video signal processing may experience baseline drift and various sources of interference; therefore, further digital filtering of this pulse wave may be necessary. Commonly used

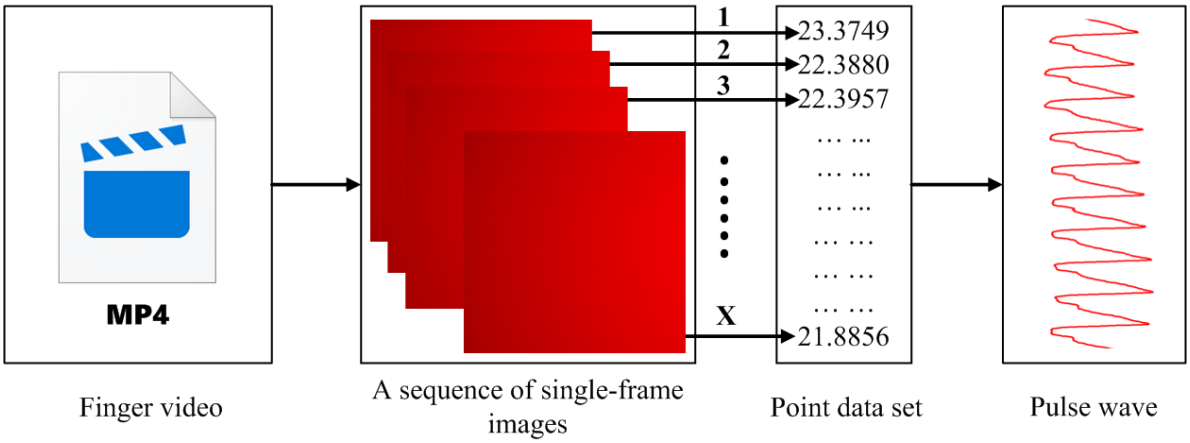

FIGURE 2. Overall diagram of the video signal processing. The acquired video signal was converted to a single-frame image sequence over time. Then, each frame image in the image sequence was transformed into point data by pixel superposition and averaging according to the space. Finally, the PPG pulse wave can be obtained by sorting these point data across time.

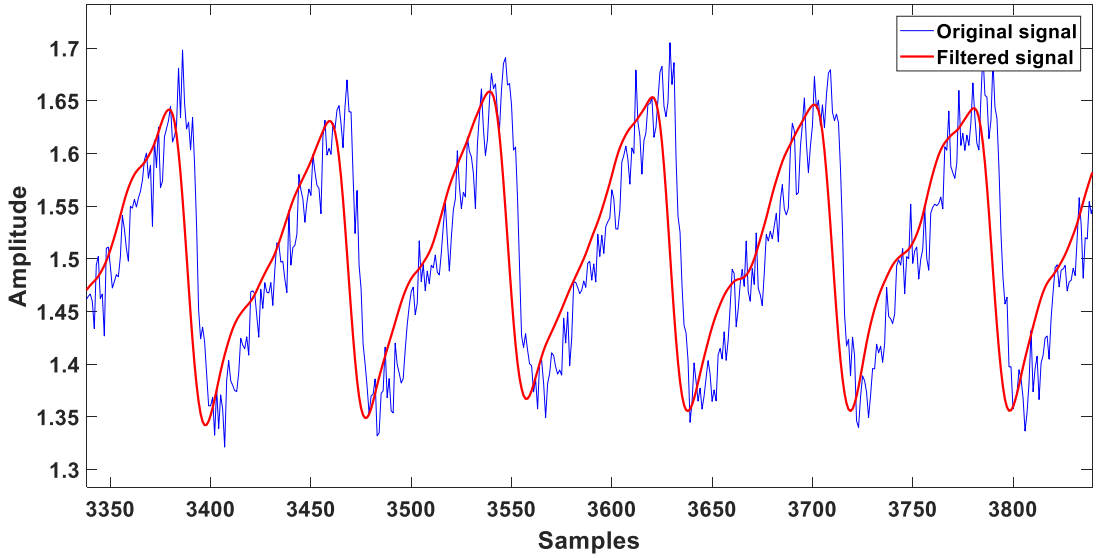

FIGURE 3. Comparison of waveforms before and after Chebyshev filtering.

digital filtering algorithms for pulse waves include wavelet filtering [27], independent component analysis (ICA) [28], Kalman filtering [29], and mathematical morphological filtering [30]. A Chebyshev type II filter [31] was used in this study. According to the passband cutoff frequency for pulse waves, stopband initial cutoff frequency, maximum passband attenuation decibel, minimum stopband attenuation decibel, and other requirements, the fluctuation coefficient and filter order was calculated. Ultimately, the system function of the filter was obtained. Figure 3 shows the waveform comparison of pulse waves before and after Chebyshev II filtering.

C. FEATURE EXTRACTION

Feature value extraction of synchronously acquired ECG signals and PPG signals is needed for the next step in the analysis. The ECG signal is used to extract the R wave and calculate its RRI time series; the PPG signal is used to extract the peak values and calculate the PPI time series (Figure 4). In the experiment, we synchronized ourselves with Beijing time. Manual checks were then performed to ensure that each pair of RRI and PPI was aligned.

The methods for extracting the feature values of the ECG and PPG signals include finite difference method [32], wavelet transform method [33], and morphological method [34]. In this study, the Hilbert transform was used for the extraction. The Hilbert transform is a linear transformation. For signal $x(t)$, the transformation [35], [36] can be defined as

$$\hat{x}(t) = H[x(t)] = \frac{1}{\pi}\int_{-\infty}^{\infty} x(\tau)\frac{1}{t-\tau}d\tau \qquad (2)$$

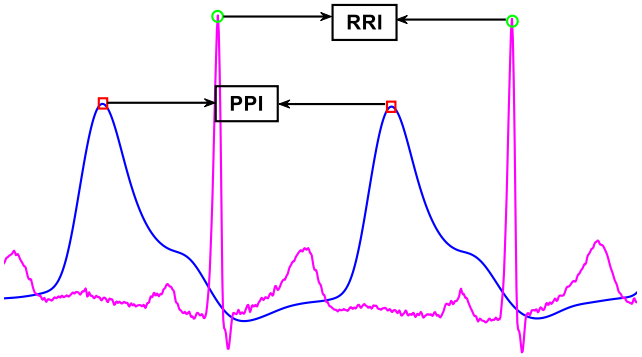

FIGURE 4. The RRI and PPI extracted from the simultaneously recorded ECG and pulse wave signals respectively. RRI is calculated based on the R to R wave of ECG. PPI is calculated from the peak to peak of the pulse wave.

Equation (2) indicates that the time-independent components remain unchanged before and after the transformation; thus, $x\ (t)$ can be expressed as the convolution form of $x\ (t)$ and $(\pi t)^{-1}$,

$$\hat{x}\ (t) = \frac{1}{\pi t} * x(t). \tag{3}$$

By performing Fourier transformations on both sides of equation (3), we obtain

$$F\left\{\hat{x}\ (\mathrm{t})\right\} = \frac{1}{\pi} F\left\{\frac{1}{t}\right\} F\left\{x\ (t)\right\}. \tag{4}$$

Because

$$F\left\{\frac{1}{t}\right\} = \int_{-\infty}^{\infty} \frac{1}{x} e^{-j2\pi fx} dx = -j\pi\,\mathrm{sgn}f \tag{5}$$

where sgn f is a sign function (i.e., 1 when $f\ >\ 0$, 0 when $f\ =\ 0$, and $-\ 1$ when $f\ <\ 0$), the Fourier transform of the Hilbert transform $x\ (t)$ from the original signal $x\ (t)$ can be expressed as

$$F\left\{\hat{x}\ (\mathrm{t})\right\} = -j\pi\,\mathrm{sgn}f F\left\{x\ (t)\right\}. \tag{6}$$

Because the Hilbert transform is an odd function, after the Hilbert transformation of the signal, the inflection point of the original signal corresponds to the zero-crossing point of its Hilbert transform signal. For the zero-crossing point, the extreme point will appear in the Hilbert transform. Using this property of the Hilbert transform, the position of the R-wave in the ECG signal or the position of the peak in the PPG signal is determined such that the RRI and PPI are calculated (Figure 5).

D. HRV ANALYSIS

The HRV time domain indices include the mean HR, maximum HR (Max HR), minimum HR (Min HR), the standard deviation of all normal-to-normal (NN) intervals (SDNN), the root mean square of the successive differences in the adjacent NN (RMSSD), the number of pairs of successive NN intervals that differ by more than 50 ms (NN50), and the proportion of NN50 divided by the total number of NN intervals (pNN50). The calculation formulas for HR, SDNN, and RMSSD are as follows [37]:

$$\mathrm{HR} = \frac{60}{RRI} \tag{7}$$

$$\mathrm{SDNN} = \sqrt{\frac{1}{N}\sum_{i=1}^{N}\left(RRI_i - \bar{RRI}\right)^2} \tag{8}$$

$$\mathrm{RMSSD} = \sqrt{\frac{1}{N-1}\sum_{i=1}^{N-1}\left(RRI_{i+1} - RRI_i\right)^2} \tag{9}$$

The HRV frequency domain parameters include very low frequency power (VLF), low frequency power (LF), high frequency power (HF), total power (TP), normalized units of LF (LFnu), normalized units of HF (HFnu), and the ratio of LF to HF (LF/HF), where VLF is defined as 0 - 0.04 Hz, LF is defined as 0.04 - 0.15 Hz, HF is defined as 0.15 - 0.5 Hz, and TP is defined as 0 - 0.5 Hz. All calculations for the power spectrum density are based on the fast Fourier transform (FFT).

Most studies use ellipse-fitting methods to analyze Poincaré plots, and short-axis SD1 and long-axis SD2 are indicators of quantitative analyses, where SD1 reflects the difference between adjacent RRIs, representing the instantaneous HR change and SD2 reflects the overall degree of variation in the HR. The calculation formulas for SD1 and SD2 are as follows [38]:

$$SD1 = \sqrt{\frac{1}{N-1}\sum_{i=1}^{N-1}\frac{\left(RRI_i - RRI_{i+1}\right)^2}{2}} \tag{10}$$

$$SD2 = \sqrt{\frac{1}{N-1}\sum_{i=1}^{N-1}\frac{\left(RRI_i + RRI_{i+1} - 2\bar{RRI}\right)^2}{2}} \tag{11}$$

In equations (8) – (11), N is the total number of all normal sinus RRIs, RRI_i and RRI_{i+1} are the ith and the $i+1$th RRIs, respectively, and $\overline{RRI}$ is the average of all N RRIs.

E. STATISTICAL ANALYSIS

Histograms of the HRV frequency domain parameters showed an obvious right skew; they were expressed as natural logarithms prior to further analyses. To assess the consistency between the two measurement methods, matched-pair tests, Pearson correlation analyses, Bland-Altman analyses, and effect sizes (ES) were used to process the data between the groups. In the Pearson correlation analyses, the correlation coefficient r was used to characterize the degree of correlation between the two sets of data; a larger absolute value of r indicated a stronger correlation. In the Bland-Altman analysis, the 95% LoA for the two sets of data was calculated as the mean of the difference between the two $\pm$ 1.96 standard deviation. The magnitude of the difference between HRV parameters was assessed using the ES with smaller values, which indicated lower differences [39]–[41]. The ES value is expressed as the difference between the means of the two samples divided by the pooled variance. The criteria for defining the magnitude of ES values included the following: the difference was small when $ES \leq 0.2$; the difference was

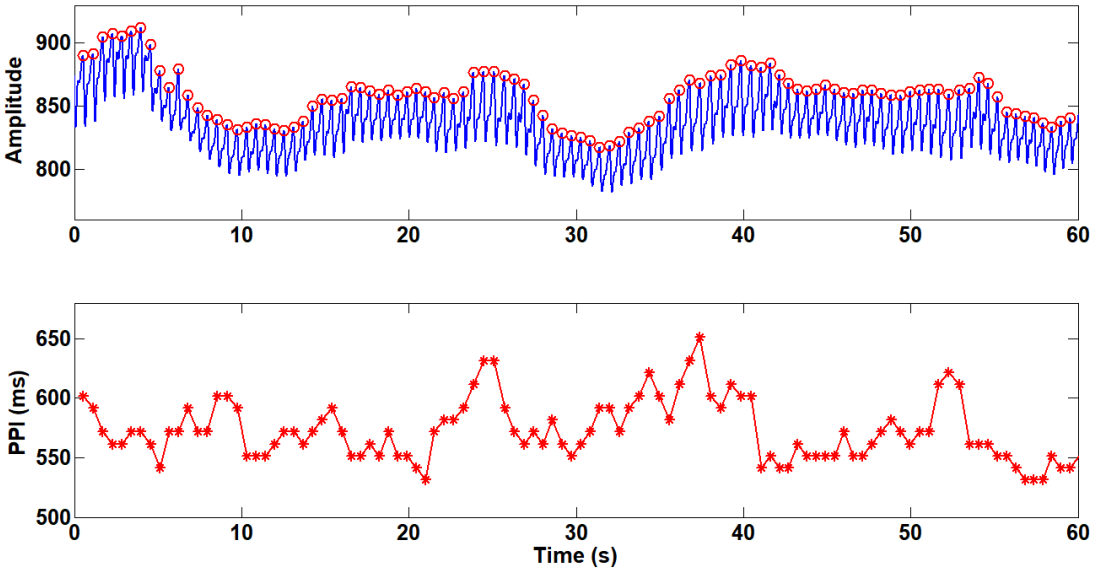

FIGURE 5. A typical PPI extraction instance.

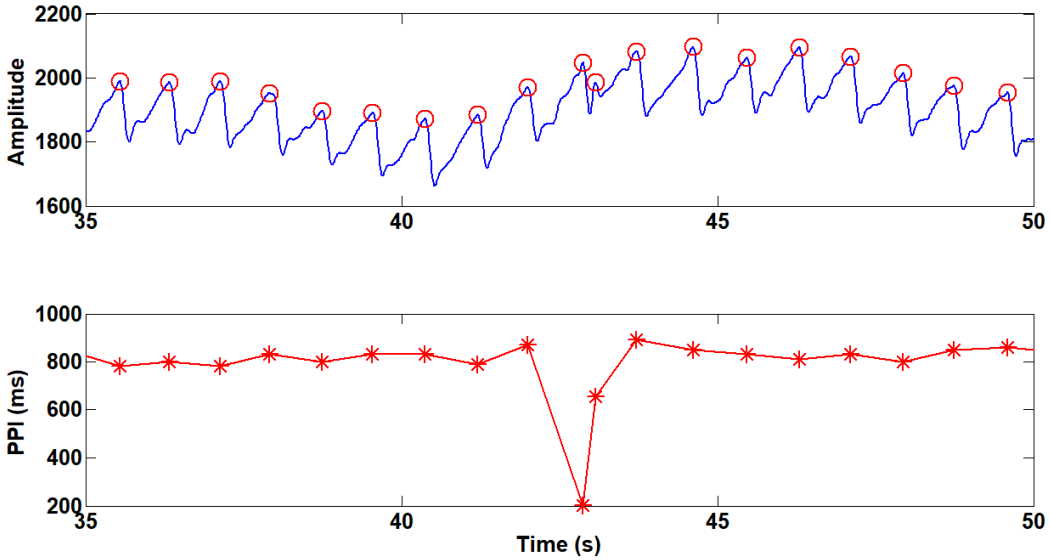

FIGURE 6. A representative illustration of PPI error detection.

moderate when $ES \leq 0.5$; and the difference was large when $ES \geq 0.8$ [42]. $p < 0.05$ was considered significant for all analyses. These analyses were performed using SPSS (ver. 23.0, SPSS, Inc., Chicago, IL., USA) statistical software and MATLAB (MathWorks, Natick, MA, USA) self-programming.

III. RESULTS

The fingertip video and ECG signals of the 24 subjects were analyzed to obtain 2114 PPIs and 2108 RRIs, respectively. Of the 2114 PPIs, there were 6 ($< 0.3\%$) misdetections. Figure 6 shows a typical example of a PPI misdetection.

The primary cause for the six false checks was interference. We addressed these false checks by adding two PPI values. In practical applications, automatic corrections can be adopted. Here, we used manual corrections. After manually correcting, a total of 2108 pairs of PPI and RRI values were obtained. There was a strong correlation between the two sets of data ($r = 0.994$, $p = 0.000$) (Figure 7). The Bland-Altman analyses showed that the mean of the difference between the two datasets was -0.2 ms, the 95% LoA range was (-19.8, 20.2) ms (Figure 8), and $ES = 0.001$, indicating a small difference.

The time domain parameters, frequency domain parameters, and Poincaré plot parameters of the HRV were analyzed for their PPI and RRI values, respectively, and the results are shown in Table 1. There was an extremely strong correlation between the two methods for all the HRV indices ($r > 0.95$,

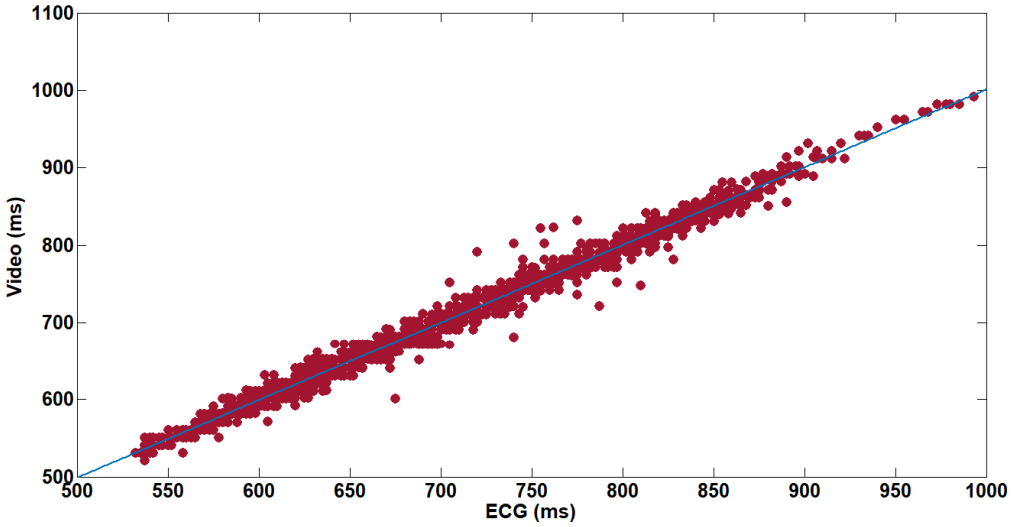

FIGURE 7. The correlation between the PPI and RRI ($r = 0.994$, $p = 0.000$).

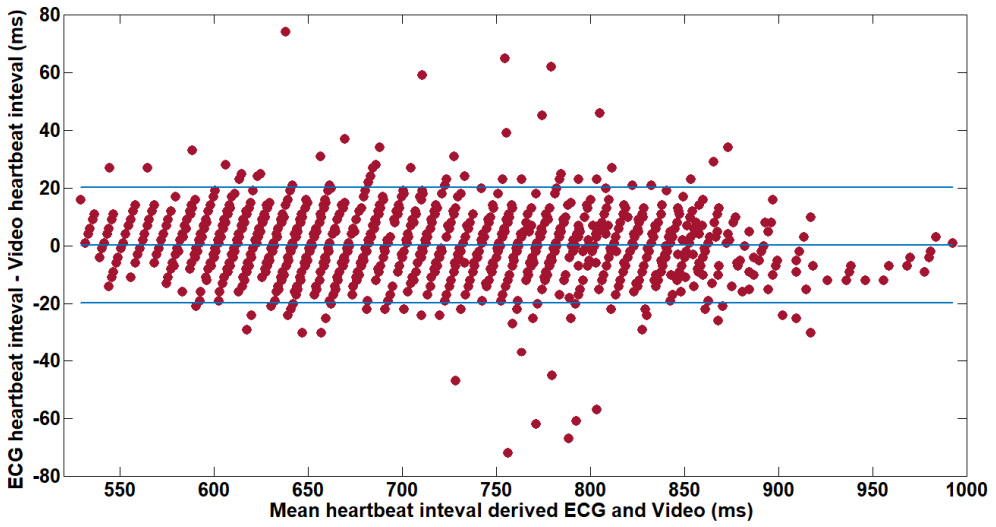

FIGURE 8. Bland-Altman agreement analysis between the PPI and RRI. The mean of the difference between the two datasets was -0.2 ms, and the 95% LoA range was (-19.8, 20.2) ms.

$p = 0.000$). Except for the RMSSD, HF, and SD1, the *ES* was small (< 0.2) for all evaluated indices between the two methods.

References [6] and [25] are more consistent with our study. In reference [6], the 14 HRV parameters from vPPG were highly correlated ($r > 0.7, p < 0.001$) with those from ECG, and only 7 of them were in the acceptable range. However, our study still has a little difference in accuracy compared with reference [25].

IV. DISCUSSION

The existing studies based on vPPG technology have primarily focused on applying this technology within the field of HR monitoring [19]–[23]. For HR monitoring, the high PPI measurement accuracy is not required but should be dynamic and in real time. Therefore, a noncontact method has generally been adopted as the measurement mode. In video signal processing, techniques such as BSS, ICA, and FFT analyses must be used to remove noise. The HRV Values are expressed as the mean (standard deviation). measurement typically does not depend on long-term continuous monitoring. In practice, it is usually performed with ECG data of <=5 minutes [7]. However, HRV measurement does require a high PPI accuracy. It is often difficult to meet the requirements using a noncontact method; therefore, a contact method has generally been adopted. Unlike the traditional noncontact video acquisition technology, BSS, ICA, and other denoising technologies are not required for collecting fingertip video signals by contact methods when the subject is in a quiet state. Instead, the spatial pixel attribute values of each frame are superimposed and averaged; then, the pulse wave signals are synthesized from a time perspective. Although there is

TABLE 1. Comparison of HRV parameters between the video and ECG.

	Video	ECG	Correlation (*r*, *P*)	Bias (LoA)	Effect size (interpretation)
Mean RR (ms)	716.3±85.7	716.5±85.6	(1.000, 0.000)	-0.2(-1.2 to 0.8)	0.002 (small)
Mean HR (BPM)	85.0±10.1	84.9±10.1	(1.000, 0.000)	0.1(-0.5 to 0.6)	0.008 (small)
Min HR (BPM)	79.0±8.8	79.0±8.8	(0.998, 0.000)	-0.1(-1.1 to 0.9)	0.009 (small)
Max HR (BPM)	92.0±11.6	91.9±11.5	(0.999, 0.000)	0.2(-0.8 to 1.1)	0.014 (small)
SDNN (ms)	38.9±13.0	36.7±12.5	(0.996, 0.000)	2.2(-0.2 to 4.6)	0.171 (small)
RMSSD (ms)	34.4±15.5	29.6±15.7	(0.983, 0.000)	4.9(0.8 to 10.6)	0.311 (moderate)
NN50	12±12	10±11	(0.962, 0.000)	2.2(-4.1 to 8.5)	0.190 (small)
pNN50 (%)	14.6±16.2	12.0±16.0	(0.970, 0.000)	2.6(-5.1 to 10.3)	0.162 (small)
LnVLF	5.046±1.149	5.048±1.121	(0.999, 0.000)	-0.001(-0.121 to 0.112)	0.001 (small)
LnLF	5.396±0.813	5.343±0.784	(0.998, 0.000)	0.053(-0.069 to 0.174)	0.066 (small)
LnHF	5.975±1.133	5.734±1.173	(0.975, 0.000)	0.241(-0.271 to 0.753)	0.209 (moderate)
LnTP	6.866±0.848	6.723±0.847	(0.989, 0.000)	0.143(-0.107 to 0.392)	0.168 (small)
LFnu (n.u.)	37.8±22.0	41.8±21.6	(0.954, 0.000)	-4.0(-17.0 to 9.1)	0.182 (small)
HFnu (n.u.)	62.1±22.0	58.1±21.5	(0.954, 0.000)	4.0(-9.0 to 17.0)	0.184 (small)
LF/HF	1.027±1.359	1.155±1.391	(0.954, 0.000)	-0.129(-0.948 to 0.691)	0.094 (small)
SD1 (ms)	24.5±11.1	21.1±11.2	(0.983, 0.000)	3.5(-0.6 to 7.5)	0.311 (moderate)
SD2 (ms)	48.6±16.2	46.7±15.5	(0.998, 0.000)	1.9(-0.5 to 4.4)	0.121 (small)

Values are expressed as the mean (standard deviation).

some noise in the pulse wave signal, it can be processed by simple digital filtering. The HRV analysis of these pulse waves showed that all indices, except RMSSD, HF, and SD1, were strongly correlated with the results of the ECG measurement with very small differences and within acceptable ranges of error. The results presented in this study confirmed the feasibility of the proposed method for HRV analysis.

The periodic systolic and diastolic heart activity causes blood to enter arteries and return from veins, forming a blood circulation system. The pulse wave is formed by the spreading of heart pulsation along arterial blood vessels and by blood flow to peripheral arteries. From a temporal perspective, the PPI lags relative to the RRI; as such, using the PPI for HRV analysis may produce errors. However, the existing research has shown that in a resting state, all of the time- and frequency-domain HRV indices analyzed with the PPI were negligibly different from those analyzed with the RRI [16]–[18]. Therefore, there are inherent errors in using PPI instead of RRI to analyze HRV. But such errors are negligible.

Another error factor is the PPI accuracy. Generally, the frame rate of a smartphone camera is approximately 25 f/s, and the sampling rate of the corresponding pulse wave after processing is 25 Hz. In this study, a 4x slow-motion mode was adopted to improve the sampling rate to 100 Hz. The sampling rate of ECG signals for HRV analysis is recommended to be no less than 250 Hz [7]. Compared with that of the RRI, the average difference for the PPI, as calculated by the method proposed in this study, was 0.2 ms, but the range for the 95% limit of agreement reached from −19.8 to 20.2 ms. Therefore, the low sampling rate may be the fundamental reason for the large differences in high-frequency indicators. For undersampled signals, interpolation is an effective method for improving the sampling rate. We performed parabolic interpolation and Fourier interpolation but had little success. The interpolation method requires further study.

Among the HRV indices, SDNN and LF represent the coregulation of sympathetic and parasympathetic nerves, and the LF/HF ratio represents the balance between the sympathetic and parasympathetic nerves [7]. The results of this study show that the SDNN and LF/HF calculated by the video technique proposed in this paper have high correlations with the ECG method to the extent that there is no significant difference between the two methods. This finding demonstrates the great potential of applying video technology in HRV analysis. To date, HRV measurement has been used to quantitatively evaluate the overall autonomic nerve activity and to track the balance of the sympathetic and parasympathetic nerves. For example, in patients with heart failure [43] and terminal illnesses [44], many variables are involved in the HRV decrease, and thus, HRV has become an independent prognostic indicator for these diseases. Unlike the traditional HRV measurement method, the method proposed in this study enables patients to use smartphones to perform remote monitoring and evaluation at home. Another example is that HRV is age related and can be used as a noninvasive biological marker for assessing aging [9]. If a big data model of HRV and age is established with this method, the quantitative assessment of daily aging can be performed and used for health guidance.

vPPG is more sensitive to interference and noise than ECG acquisition. Therefore, there are several obvious limitations to this study. First, differences in skin tones, skin roughness, and even fat thickness affected the absorption and reflection of light to some extent, thus affecting the quality of the PPG signal. Therefore, the influence of these factors on the accuracy of the HRV measurement should be further explored. Second, due to the influence of subjective and objective factors, such as the size of the phone, the size of the individual's

palm, and the degree of personal tension, the pressure on the fingers of each person varied. Pressure intensity and stability greatly influence the PPG signal quality. In extreme cases, the pulse wave shape may not even be obtained and thus may need to be measured again. Therefore, further research is needed to address this issue. Third, although we preliminarily verified that this method can be used for quantitative evaluations of personal daily ANS values, it is necessary to further study the ANS level of subjects under different stress states and evaluate whether the device can capture these changes.

V. CONCLUSION

We proposed a new method for HRV analysis based on the rear-facing camera of a smartphone. This method abandons traditional signal separation and time-frequency transformation methods; instead, this method uses the time-space-time transformation of the video signal to obtain the PPG and then applies the Hilbert transform to calculate the PPI for HRV analysis. There was a very strong correlation with the RRI and HRV parameters obtained using the ECG method. Except for RMSSD, HF, and SD1, the differences for all indices were very small. These findings suggest that this method can be used to quantitatively assess the overall activity and balance of autonomic nerves and for the quantitative management of an individual's day-to-day health. Future directions will include the development of applications based on a smartphone platform.

REFERENCES

[1] M. Elsherif, M. U. Hassan, A. K. Yetisen, and H. Butt, "Wearable contact lens biosensors for continuous glucose monitoring using smartphones," *ACS Nano*, vol. 12, no. 6, pp. 5452–5462, May 2018.

[2] Q. Liu, H. Yuan, Y. Liu, J. Wang, Z. Jing, and W. Peng, "Real-time biodetection using a smartphone-based dual-color surface plasmon resonance sensor," *Proc. SPIE*, vol. 23, no. 4, Apr. 2018, Art. no. 047003.

[3] J. A. Taylor, J. W. Stout, L. de Greef, M. Goel, S. Patel, E. K. Chung, A. Koduri, S. Mcmahon, J. Dickerson, E. A. Simpson, and E. C. Larson, "Use of a smartphone app to assess neonatal jaundice," *Pediatrics*, vol. 140, no. 3, Sep. 2017, Art. no. e20170312.

[4] A. Chandrasekhar, C.-S. Kim, M. Naji, K. Natarajan, J.-O. Hahn, and R. Mukkamala, "Smartphone-based blood pressure monitoring via the oscillometric finger-pressing method," *Sci. Transl. Med.*, vol. 10, no. 431, Mar. 2018, Art. no. eaap8674.

[5] F. Miao, Y. Cheng, Y. He, Q. He, and Y. Li, "A wearable context-aware ECG monitoring system integrated with built-in kinematic sensors of the smartphone," *Sensors*, vol. 15, no. 5, pp. 11465–11484, May 2015.

[6] R.-C. Peng, X.-L. Zhou, W.-H. Lin, and Y.-T. Zhang, "Extraction of heart rate variability from smartphone photoplethysmograms," *Comput. Math. Methods Med.*, vol. 2015, Jan. 2015, Art. no. 516826.

[7] Task Force of the European Society of Cardiology and the North American Society of Pacing and Electrophysiology, "Heart rate variability: Standards of measurement, physiological interpretation, and clinical use," *Circulation.*, vol. 93, no. 5, pp. 1043–1065, Mar. 1996.

[8] A. Voss, A. Heitmann, R. Schroeder, A. Peters, and S. Perz, "Short-term heart rate variability—Age dependence in healthy subjects," *Physiol. Meas.*, vol. 33, no. 8, pp. 1289–1311, Aug. 2012.

[9] A. Voss, R. Schroeder, A. Heitmann, A. Peters, and S. Perz, "Short-term heart rate variability—Influence of gender and age in healthy subjects," *PLoS ONE*, vol. 10, no. 3, Mar. 2015, Art. no. e0118308.

[10] K. Shin, H. Minamitani, S. Onishi, H. Yamazaki, and M. Lee, "The power spectral analysis of heart rate variability in athletes during dynamic exercise—Part I," *Clin. Cardiol.*, vol. 18, no. 10, pp. 583–586, Oct. 1995.

[11] X. Wang, C. Yan, B. Shi, C. Liu, C. Karmakar, and P. Li, "Does the temporal asymmetry of short-term heart rate variability change during regular walking? A pilot study of healthy young subjects," *Comput. Math. Methods Med.*, vol. 2018, Apr. 2018, Art. no. 3543048.

[12] C. R. Cardoso, R. A. Moraes, N. C. Leite, and G. F. Salles, "Relationships between reduced heart rate variability and pre-clinical cardiovascular disease in patients with type 2 diabetes," *Diabetes Res. Clin. Pract.*, vol. 106, no. 1, pp. 110–117, Oct. 2014.

[13] H. Mussalo, E. Vanninen, R. Ikäheimo, T. Laitinen, M. Laakso, E. Länsimies, and J. Hartikainen, "Heart rate variability and its determinants in patients with severe or mild essential hypertension," *Clin. Physiol.*, vol. 21, no. 5, pp. 594–604, Sep. 2001.

[14] S. Hu, J. Lou, Y. Zhang, and P. Chen, "Low heart rate variability relates to the progression of gastric cancer," *World J. Surgical Oncol.*, vol. 16, no. 1, p. 49, Mar. 2018.

[15] J. Moraes, M. Rocha, G. Vasconcelos, J. V. Filho, V. de Albuquerque, and A. Alexandria, "Advances in photopletysmography signal analysis for biomedical applications," *Sensors*, vol. 18, no. 6, p. 1894, Jun. 2018.

[16] N. Selvaraj, A. Jaryal, J. Santhosh, K. K. Deepak, and S. Anand, "Assessment of heart rate variability derived from finger-tip photoplethysmography as compared to electrocardiography," *J. Med. Eng. Technol.*, vol. 32, no. 6, pp. 479–484, Jan. 2008.

[17] G. Lu, F. Yang, J. A. Taylor, and J. F. Stein, "A comparison of photoplethysmography and ECG recording to analyse heart rate variability in healthy subjects," *J. Med. Eng. Technol.*, vol. 33, no. 8, pp. 634–641, Dec. 2009.

[18] E. Gil, M. Orini, R. Bailón, J. M. Vergara, L. Mainardi, and P. Laguna, "Photoplethysmography pulse rate variability as a surrogate measurement of heart rate variability during non-stationary conditions," *Physiol. Meas.*, vol. 31, no. 9, pp. 1271–1290, Aug. 2010.

[19] M. Z. Poh, D. J. McDuff, and R. W. Picard, "Non-contact, automated cardiac pulse measurements using video imaging and blind source separation," *Opt. Exp*, vol. 18, no. 10, pp. 10762–10774, May 2010.

[20] K. Matsumura and T. Yamakoshi, "IPhysioMeter: A new approach for measuring heart rate and normalized pulse volume using only a smartphone," *Behav. Res. Methods*, vol. 45, no. 4, pp. 1272–1278, Dec. 2013.

[21] S. A. Siddiqui, Y. Zhang, Z. Feng, and A. Kos, "A pulse rate estimation algorithm using PPG and smartphone camera," *J. Med. Syst.*, vol. 40, no. 5, p. 126, May 2016.

[22] J.-P. Lomaliza and H. Park, "A highly efficient and reliable heart rate monitoring system using smartphone cameras," *Multimedia Tools Appl.*, vol. 76, no. 20, pp. 21051–21071, Oct. 2016.

[23] R. Zaman, C. H. Cho, K. Hartmann-Vaccarezza, T. N. Phan, G. Yoon, and J. W. Chong, "Novel fingertip image-based heart rate detection methods for a smartphone," *Sensors*, vol. 17, no. 2, pp. 358–370, Feb. 2017.

[24] R.-Y. Huang and L.-R. Dung, "Measurement of heart rate variability using off-the-shelf smart phones," *Biomed. Eng. OnLine*, vol. 15, no. 1, pp. 1–16, Jan. 2016.

[25] A. Bánhalmi, J. Borbás, M. Fidrich, V. Bilicki, Z. Gingl, and L. Rudas, "Analysis of a pulse rate variability measurement using a smartphone camera," *J. Healthcare Eng.*, vol. 2018, Art. no. 4038034, Feb. 2018.

[26] T. Thap, H. Chung, C. Jeong, J. Ryu, Y. Nam, K.-H. Yoon, and J. Lee, "Real-time heart activity monitoring with optical illusion using a smartphone," *Multimedia Tools Appl.*, vol. 77, no. 5, pp. 6209–6224, Mar. 2018.

[27] T.-H. Fu, S.-H. Liu, and K.-T. Tang, "Heart rate extraction from photoplethysmogram waveform using wavelet multi-resolution analysis," *J. Med. Biol. Eng.*, vol. 28, no. 4, pp. 229–232, Dec. 2008.

[28] M. Granegger, T. Werther, and H. Gilly, "Use of independent component analysis for reducing CPR artefacts in human emergency ECGs," *Resuscitation*, vol. 82, no. 1, pp. 79–84, Jan. 2011.

[29] M. H. Moradi, M. A. Rad, and R. B. Khezerloo, "ECG signal enhancement using adaptive Kalman filter and signal averaging," *Int. J. Cardiol.*, vol. 173, no. 3, pp. 553–555, May 2014.

[30] C.-H.-H. Chu and E. J. Delp, "Impulsive noise suppression and background normalization of electrocardiogram signals using morphological operators," *IEEE Trans. Biomed. Eng.*, vol. 36, no. 2, pp. 262–273, Feb. 1989.

[31] L. J. Karam and J. H. McClellan, "Chebyshev digital FIR filter design," *Signal Process.*, vol. 76, no. 1, pp. 17–36, Jul. 1999.

[32] B. N. Li, M. C. Dong, and M. I. Vai, "On an automatic delineator for arterial blood pressure waveforms," *Biomed. Signal Process. Control*, vol. 5, no. 1, pp. 76–81, Jan. 2010.

[33] S. Mallat and W. L. Hwang, "Singularity detection and processing with wavelets," *IEEE Trans. Inf. Theory*, vol. 38, no. 2, pp. 617–643, Mar. 1992.

[34] P. E. Trahanias, "An approach to QRS complex detection using mathematical morphology," *IEEE Trans. Biomed. Eng.*, vol. 40, no. 2, pp. 201–205, Feb. 1993.
[35] R. N. Bracewell, *The Fourier Transform and Its Applications*. New York, NY, USA: McGraw-Hill, 1978, pp. 267–274.
[36] D. Benitez, P. A. Gaydecki, A. Zaidi, and A. P. Fitzpatrick, "The use of the Hilbert transform in ECG signal analysis," *Comput. Biol. Med.*, vol. 31, no. 5, pp. 399–406, Sep. 2001.
[37] C. A. G. Martinez, "Time-domain analysis," in *Heart Rate Variability Analysis With the R Package RHRV*. Cham, Switzerland: Springer, 2017, ch. 3, sec. 1, pp. 29–32.
[38] A. H. Khandoker, "Quantitative Poincaré plot," in *Poincaré Plot Methods for Heart Rate Variability Analysis*. New York, NY, USA: Springer, 2013, ch. 2, sec. 3, pp. 15–18.
[39] D. Giles, N. Draper, and W. Neil, "Validity of the polar V800 heart rate monitor to measure RR intervals at rest," *Eur. J. Appl. Physiol.*, vol. 116, no. 3, pp. 563–571, Mar. 2016.
[40] D. A. Giles and N. Draper, "Heart rate variability during exercise: A comparison of artefact correction methods," *J. Strength Conditioning Res.*, vol. 32, no. 3, pp. 726–735, Mar. 2018.
[41] P. Caminal, F. Sola, P. Gomis, E. Guasch, A. Perera, N. Soriano, and L. Mont, "Validity of the polar V800 monitor for measuring heart rate variability in mountain running route conditions," *Eur. J. Appl. Physiol.*, vol. 118, no. 3, pp. 669–677, Mar. 2018.
[42] J. Cohen, "The T-test for means," in *Statistical Power Analysis for the Behavioral Sciences*, 2nd ed. Mahwah, NJ, USA: Lawrence Erlbaum Associates, 1988, pp. 20–40.
[43] K. Imai, H. Sato, M. Hori, H. Kusuoka, H. Ozaki, H. Yokoyama, H. Takeda, M. Inoue, and T. Kamada, "Vagally mediated heart rate recovery after exercise is accelerated in athletes but blunted in patients with chronic heart failure," *J. Amer. College Cardiol.*, vol. 24, no. 6, pp. 1529–1535, Nov. 1994.
[44] C. Arab, D. P. M. Dias, R. T. D. A. Barbosa, T. D. D. Carvalho, V. E. Valenti, T. B. Crocetta, M. Ferreira, L. C. D. Abreu, and C. Ferreira, "Heart rate variability measure in breast cancer patients and survivors: A systematic review," *Psychoneuroendocrinology*, vol. 68, pp. 57–68, Jun. 2016.

GENXUAN ZHANG received the M.S. degree in circuits and systems from Anhui University, Hefei, China, in 2007.

He is currently an Associate Professor with the School of Medical Imaging, Bengbu Medical College, Bengbu, China. His research interests include biomedical signal processing and analysis. He has published over ten research articles on these topics.

SAI ZHANG received the B.S. degree in electronic information science and technology from Tianjin Chengjian University, Tianjin, China, in 2013, and the M.S. degree in circuits and systems from the Anhui University of Science and Technology, Huainan, China, in 2016.

She is currently a Lecturer with the School of Medical Imaging, Bengbu Medical College, Bengbu, China. Her research interests include biomedical signal acquisition and analysis.

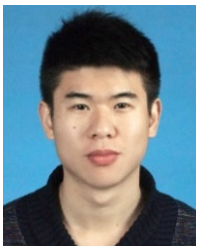

YIMING DAI received the B.S. degree in electronic and information engineering from Hefei Normal University, Hefei, China, in 2012, and the M.S. degree in electromagnetic and microwave technology from Anhui University, Hefei, in 2015.

He is currently a Lecturer with the School of Medical Imaging, Bengbu Medical College, Bengbu, China. His research interest includes biomedical signal analysis.

BO SHI received the B.S. degree in electronic science and technology from Xuzhou Normal University, Xuzhou, China, in 2004, and the M.S. degree in biomedical engineering from the Nanjing University of Science and Technology, Nanjing, China, in 2006.

He is currently an Associate Professor with the School of Medical Imaging, Bengbu Medical College, Bengbu, China. His research interests include novel biomedical instrumentation, physiological measurements, and biomedical signal processing.